SPACE VECTOR MODULATION –An Introduction

== Tutorial at IECON2001==

Dorin O. Neacsu

Correspondence Address: Satcon Corporation, 161 First Street, Cambridge, MA 02142, **Email** neacsu@earthlink.net

I. INTRODUCTION

Space Vector Modulation became a standard for the switching power converters and important research effort has been dedicated to this topic. Tens of papers, research reports and patents were developed in the last ten years and the theory of Space Vector Modulation is already well-established. Diverse implementation methods were tried and some dedicated hardware pieces were developed based on this principle. The initial use of Space Vector Modulation at three-phase voltage-source inverters has been expanded by application to novel three-phase topologies as AC/DC Voltage Source Converter, AC/DC or DC/AC Current Source Converters, Resonant Three-Phase Converters, B4-inverter, Multilevel Converters, AC/AC Matrix Converters, and so on). This tutorial presents the base theory of SVM when applied to a 3-phase voltage source inverter.

II. REVIEW OF SPACE VECTOR THEORY

A. History

The roots of vectorial representation of three-phase systems are presented in the research contributions of *Park* [1] and *Kron* [2], but the decisive step on systematically using the Space Vectors was done by *Kovacs* and *Racz* [3]. They provided both mathematical treatment and a physical description and understanding of the drive transients even in the cases when machines are fed through electronic converters.

In early seventies, Space Vector theory was already widely used by industry and presented in numerous books. *Stepina* [4] and *Serrano-Iribarnegaray* [5] suggested that the correct designation for the analytical tool to analyzing electrical machines has to be "Space Phasor" instead of "Space Vector". "Space Phasor" concept is nowadays mainly used for current and flux in analysis of electrical machines.

B. Theory

Any three-phase system (defined by $a_x(t)$, $a_y(t)$ $a_z(t)$) can be represented uniquely by a rotating vector $\underline{a_S}$:

$$\underline{a_S} = \frac{2}{3}\cdot\left[a_X(t) + \underline{a}\cdot a_Y(t) + \underline{a^2}\cdot a_Z(t)\right] \qquad (1)$$

where $\underline{a} = e^{j\cdot\frac{2\pi}{3}}$ and $\underline{a^2} = e^{j\frac{4\pi}{3}}$

Given a three-phase system, the vectorial representation is achieved by the following 3/2 transformation:

$$\begin{bmatrix} A_\alpha \\ A_\beta \end{bmatrix} = \frac{2}{3}\cdot\begin{bmatrix} 1 & \frac{-1}{2} & \frac{-1}{2} \\ 0 & \frac{\sqrt{3}}{2} & \frac{-\sqrt{3}}{2} \end{bmatrix}\cdot\begin{bmatrix} a_X \\ a_Y \\ a_Z \end{bmatrix} \qquad (2)$$

where (A_α , A_β) are forming an orthogonal 2-phase system and $\underline{a_S} = A_\alpha + j\cdot A_\beta$. A vector can be uniquely defined in the complex plane by these components.

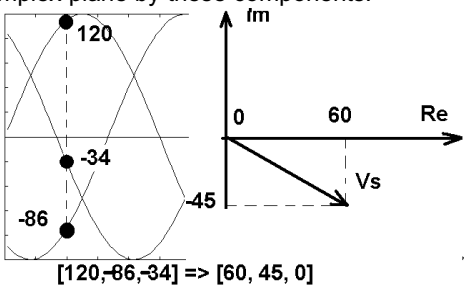

Fig.1 Equiv. between the 3-ph system and vectorial presentation

The reverse transformation (2/3 Transformation) is given by

$$\begin{cases} a_X(t) = \mathrm{Re}\left[\underline{a_S}\right] + a_0(t) \\ a_Y(t) = \mathrm{Re}\left[\underline{a^2}\cdot\underline{a_S}\right] + a_0(t) \\ a_Z(t) = \mathrm{Re}\left[\underline{a}\cdot\underline{a_S}\right] + a_0(t) \end{cases} \qquad (3) \text{ where}$$

$a_0(t) = \frac{1}{3}\cdot\left[a_X(t) + a_Y(t) + a_Z(t)\right]$ represents the homopolar component.

It results an unique correspondence between a Space Vector in the complex plane and a three-phase system. The main advantages of this mathematical representation are:

- Analysis of three-phase systems as a whole instead of looking at each phase;
- It allows to use the properties of the vectorial rotation. Using rotation with ωt leads to an analysis in DC components by withdrawing the rotational effect.

This vectorial representation is the basis for control algorithms in :

- electrical drives (Induction Machine or Synchronous Machine drives);
- AC/DC converters:
- Active filtering systems based on the instantaneous power components (*p-q*) theory.

All these control methods are based on vectorial mathematical models and are using PWM algorithms in the final control stage before the power converter.

III. VECTORIAL ANALYSIS OF THE THREE-PHASE INVERTER

A. Theory

The three-phase inverter presented in Fig.2 is herein considered. Fig.3 presents the appropriate output voltages without PWM (six-step).

IEEE Copyright 2001

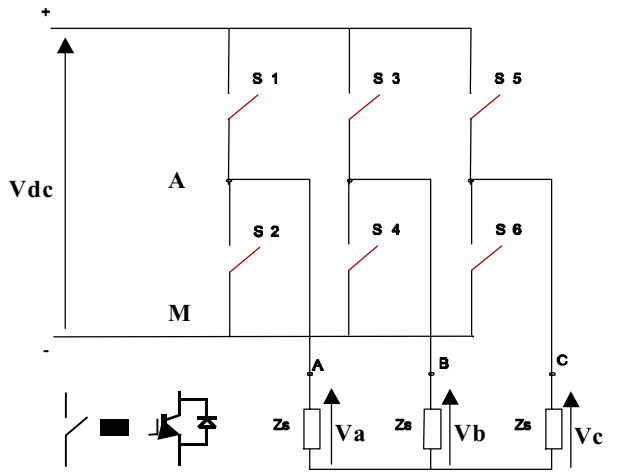

Fig.2 Three-phase voltage-source inverter

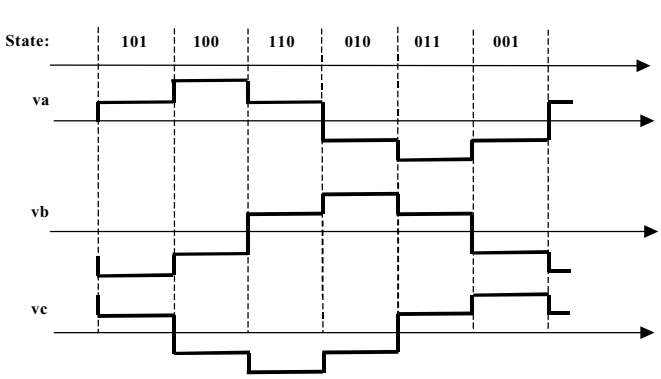

Fig.3 Output voltage waveforms and state coding for the case without PWM

Each state of the output voltage system leads to a switching vector in the complex plane. It results 6 active switching vectors V1…V6 and 2 vectors corresponding to the zero states. The magnitude of the active vectors is *(2/3)Vdc*. Since the output voltages are at 2π/3 out of phase each other, the Space Vectors system can occupy a number of positions with an order multiple of three.

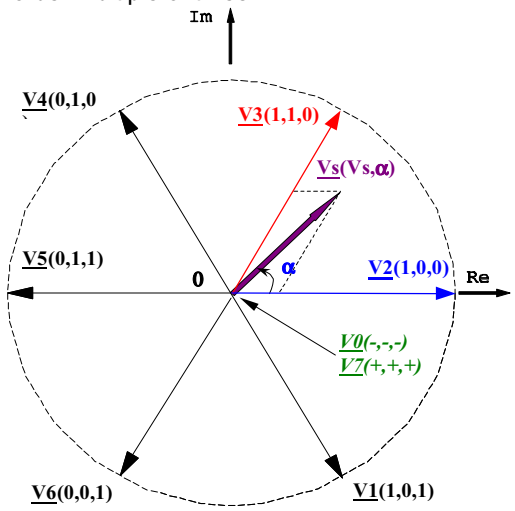

Fig.4 Switching vectors corresponding to the unmodulated operation of the inverter

The vectorial analysis of this system is first developped for an inductive three-phase load. The phase current can be derived by the integral of the phase voltage equation:

$$v_s = L \cdot \frac{di_s}{dt} \qquad (4)$$

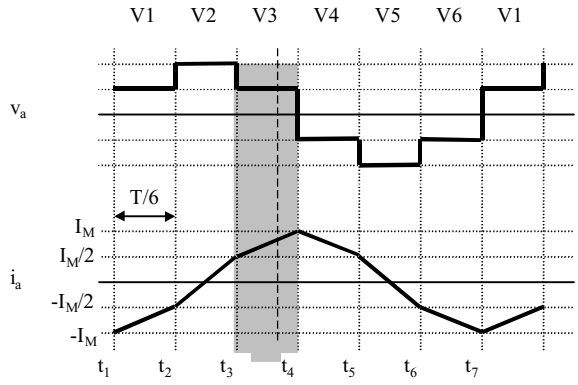

Fig.5 Output phase current waveforms

The variation slope of the phase current is doubled when the phase voltage gets doubled. The maximum value of the phase current is herein denoted with I_M. During the time interval [t3, t4], the output voltage vector is V3. Choosing the time origin in t3 (at t3=0), the load currents and voltages can be mathematically expressed from Figs.3 and 5:

$$v_a = \frac{1}{3} \cdot V_d \quad v_b = \frac{1}{3} \cdot V_d \quad v_c = -\frac{2}{3} \cdot V_d \qquad (5)$$

$$\begin{aligned} i_a(t) &= 0.5 \cdot I_M + \frac{V_d}{3 \cdot L} \cdot t \\ i_b(t) &= -I_M + \frac{V_d}{3 \cdot L} \cdot t \\ i_c(t) &= 0.5 \cdot I_M - \frac{2 \cdot V_d}{3 \cdot L} \cdot t \end{aligned} \qquad (6)$$

The Space Vectors associated to the current and voltage waveforms are given by:

$$\underline{v}(t) = \frac{2}{3} \cdot \left[v_a(t) + \underline{a} \cdot v_b(t) + \underline{a}^2 \cdot v_c(t) \right] \qquad (7)$$

$$\underline{i}(t) = \frac{2}{3} \cdot \left[i_a(t) + \underline{a} \cdot i_b(t) + \underline{a}^2 \cdot i_c(t) \right] \qquad (8)$$

where

$$\underline{a} = -\frac{1}{2} + j \cdot \frac{\sqrt{3}}{2} \quad \underline{a}^2 = -\frac{1}{2} - j \cdot \frac{\sqrt{3}}{2} \qquad (9)$$

This leads to:

$$\underline{v}(t) = \frac{2}{3} \cdot V_d + j \cdot 0 \qquad (10)$$

and

$$\underline{i}(t) = \left[\frac{I_M}{2} + \frac{1}{3} \cdot \frac{V_d}{L} \cdot t \right] + j \cdot \left[\frac{\sqrt{3}}{2} \cdot I_M + \frac{\sqrt{3} \cdot V_d \cdot t}{2 \cdot L} \right] \qquad (11)$$

The maximum value of the current (I_M) can be obtained from the current vector definition equation written for the time interval [t3, t4] and taking into account the linear variation of the phase current i_a due to the inductive load:

IEEE Copyright 2001

$$I_M = \frac{2}{3L} \cdot \frac{T}{6} \cdot V_d \quad (12)$$

The voltage Space Vector $\underline{v}(t)$ is obtained from the projection of eq.(10) on the ***Re*** and ***Im*** axes and from their composition. It can be concluded that the voltage Space Vector $\underline{v}(t)$ coincides with the switching vector that has generated it.

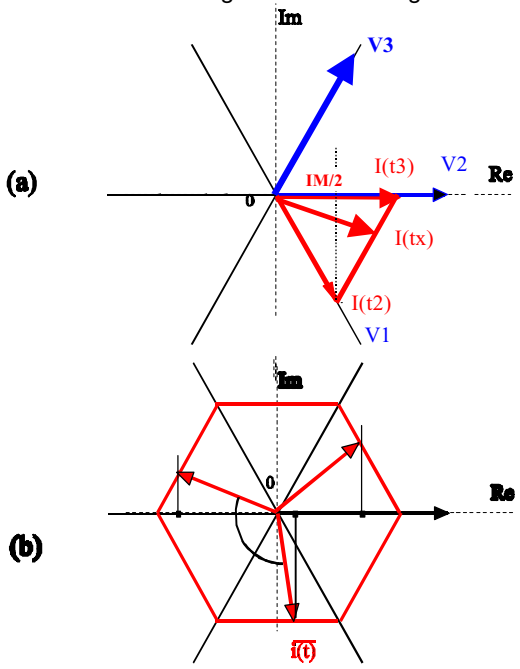

Fig.6 Current vector trajectory in the complex plane

What concerns the current Space Vector $\underline{i}(t)$, the ***Real*** part is varying linearly from $0.5I_M$ to I_M during the time interval $[t_3, t_4]$ of duration T/6. These two values of the ***Real*** part at the time moments t_3 and t_4 are calculated by substituting on the left term of the eq.(11), the time variable (t) with t_3=0 and t_4=T/6. ***Imag*** varies from $-0.866I_M$ to 0. The current Space Vector will move continuously during the time interval [t3, t4] starting from a position along the direction of V1 vector and arriving to a position along the V2 vector. In conclusion, applying the vector V3 on the load leads to a curent Space Vector trajectory as presented in Fig.6a. The vector projection on the ***Real*** axis represents the value of the first phase current.

During the next time interval [t4, t5], the voltage Space Vector is identical with the switching vector V4 that is producing the load voltages. The current Space Vector will move between the position along the vector V3 (at t4) and the position along with the vector V4 (at t5). This trajectory is also a straight line as in previous case.

The same reasoning for all six intervals leads to the conclusion that the voltage Space Vector has a discrete movement in the complex plane between positions equally partitioning 60 degrees sectors. It equals the switching vector that was producing it. The current Space Vector is describing a hexagonal trajectory in the complex plane as presented by Fig.6b. The currents on the two other axes can be defined by applying the graphical representation of the Park transform that consists in projecting the current space vector on axes at 120 and 240 degrees. By this, precise information about the phase currents can be revealed from the vectorial analysis. Moreover, due to the 60 degrees symmetry of the trajectory it is enough to limit the vectorial analysis on a 60 degrees sector.

In the general case of a three-phase R-L load, the current Space Vector can be defined by analyzing each voltage switching vector effect. The voltage Space Vector is constant and the load is characterized by:

$$\underline{V} = \underline{i} \cdot R + L \cdot \frac{d}{dt}\underline{i} \text{ with solution } \underline{i}(t) = \frac{1}{R} \cdot \underline{V} \cdot \underline{C} \cdot e^{\frac{-t}{\tau}} \quad (13)$$

where C is a complex constant and $\tau = \frac{R}{L}$ represents the time constant of the load. Supposing the initial value as being equal to ***$\underline{i}(0)=\underline{I}$*** , the current space vector will be $\underline{i}\left[\frac{\pi}{3\omega}\right] = \underline{I} \cdot e^{\frac{j\pi}{3}}$. Considering the limit conditions defines ***$\underline{C}$***:

$$\left.\begin{array}{l} t = 0 \Rightarrow \underline{I} = \frac{1}{R} \cdot \underline{V} + \underline{C} \\ t = \frac{\pi}{3} \Rightarrow \underline{I} \cdot e^{\frac{\pi}{3}} = \frac{1}{R} \cdot \underline{V} + \underline{C} \cdot e^{\frac{-\pi}{3\omega t}} \end{array}\right\} \Rightarrow$$

$$\left\{\begin{array}{l} \underline{C} = \underline{I} - \frac{1}{R} \cdot \underline{V} \\ \underline{I} \cdot e^{\frac{\pi}{3}} = \frac{1}{R} \cdot \underline{V} + \underline{C} \cdot e^{\frac{-\pi}{3\omega t}} \end{array}\right. \Rightarrow \ldots \Rightarrow \underline{i}(t) = \frac{1}{R} \cdot \underline{V} \cdot \left[1 - e^{\frac{-t}{\tau}}\right] + \underline{I} \cdot e^{\frac{-t}{\tau}}$$

where $\underline{I} = \frac{1}{R} \cdot \underline{V} \cdot \frac{1 - e^{\frac{-\pi}{3\omega t}}}{e^{\frac{j\pi}{3}} - e^{\frac{-\pi}{3\omega t}}}$ (15)

Decomposing the current Space Vector expression on the ***Real*** and ***Imag*** axes helps us to demonstrate that the current vector trajectory is a continuous function during each time interval for which the voltage is constant. Since the voltage Space Vector changes its position on discrete positions at each 60 degrees, the current Space Vector trajectory results close to hexagonal for large inductances. This is presented in Fig.7a.The effect of pulse width modulation is shown in Fig.7b.

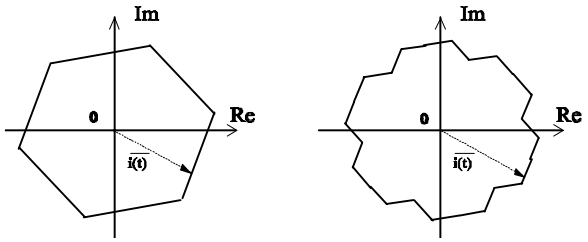

Fig.7 Current Space Vector trajectory for unmodulated inverter operation (a) and for the simplified PWM case.

IV. WHAT IS PULSE-WIDTH MODULATION?

The control of electric power is performed using power converters. The converters transfer energy from a source in a switched operation mode that ensures high efficiency of the

IEEE Copyright 2001

conversion. The algorithms that generates the switching functions are called **Pulse-Width Modulation** techniques.

In the AC/DC conversion case, it is obvious that the line inductances are acting as a LPF for the applied voltage. Considering an AC drive, the machine inductance is accounting for LPF-ing of the harmonics provided by the discontinuous power flow at switching. The flux linkage in the machine's windings is approximately equal to the time integral of the impressed voltage if voltage drops across resistance and leakage inductance of the stator windings are neglected. The flux vector yields:

$$\lambda = \int \bar{V} dt \qquad (16)$$

The flux linkage λ is intended to be kept constant in usual applications. Since ***V*** occupies different discrete positions in the complex plane, its time integral leads to a polygon close to a circle. The torque ripple has a close relationship to the deviation from a circular locus of an ideal rotational flux linkage vector λ_0. The difference between λ_0 and λ produced by a PWM inverter causes the torque pulsations. The dependence of the torque pulsation on radial and angular components of the flux error has been analyzed or presented in [11-15] and it was stated that the torque pulsation is more affected by the angular error than the radial error. The angular errors can be reduced by distributing more zero-vector states on the locus of λ so that the rotating speed becomes smoother and angular error approaches zero. The radial errors can be reduced by establishing an optimal polygonal flux locus. In conclusion, the torque ripple results lower when a higher carrier frequency (more zero vector states) is employed even if this is splitting a polygonal flux locus with a reduced number of edges. The limitation of switching frequency is desired due to the switching loss. This tradeoff is the base for defining a PWM algorithm. Due to the complexity of the control and due to the Vector Control inference requirements, digital implementation is prefered.

Different PWM produce different effects on converter load. Performance indices are defined in respect with the modulation index $m = \dfrac{V_s}{\frac{2}{3}\cdot V_{dc}}$ (17)

Most used performance indices are:

- **Content in fundamental** (***z***) represents the ratio between the RMS value of the fundamental of the output phase voltage (V_{L1}) and the RMS value of the output phase voltage (V_L). It is used mostly in Europe.
- **Total Harmonic Distortion (THD)** coefficient :

$$THD_V = \frac{\sqrt{V_L^2 - V_{L1}^2}}{V_{L1}} \qquad (6)$$

- **Harmonics of the load current** are given by:

$$I_{(n)} = \frac{V_{(n)}}{2\cdot\pi\cdot n\cdot f\cdot L_L} \qquad (7)$$

- **Percentage of the unwanted harmonics**

$$\delta = \frac{100}{I_{(1)}}\cdot\sqrt{\sum_{n=5}^{\infty} I^2{}_{(n)}} = \frac{K_1}{2\cdot\pi\cdot L_L\cdot I_{(1)}}\cdot\frac{100}{V_{(1)}}\cdot\sqrt{\sum_{n=5}^{\infty}\left[\frac{V_{(n)}}{n}\right]^2} = const.\cdot HCF$$

- **Harmonic Current Factor (HCF)** – is mainly dedicated to motor drives where the load is strongly inductive and will filter out the voltage harmonics.

$$HCF(\%) = \frac{100}{V_{(1)}}\cdot\sqrt{\sum_{n=5}^{\infty}\left[\frac{V_{(n)}}{n}\right]^2} \qquad (9)$$

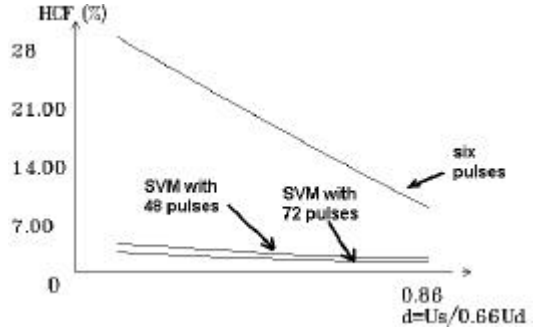

Fig.8 Example of HCF variation for synchronized SVM and six-step operation

- **Current distorsion factor**

$$DF = \frac{I_{harm,rms}}{I_{harm,6-step}} \qquad (10)$$

This performance index is equivalent with HCF.

- **Current distortion factor (2)**

The constraints for high-power uninterruptable power supplies UPS (constant frequency, variable-voltage) consists of low output impedance and less than 5% total harmonic distortion voltage content (THD) at load terminals. An output LC filter is necessary to decrease the THD content of the output voltage. Denoting the harmonics of the filter output voltage by V_n^*, THD is well-known as in eq.(6). Taking into account the effect of the filter and the transfer function between the output voltage and the inverter voltage, THD becomes proportional with:

$$DF^2 = \frac{100}{V1}\bullet\sqrt{\sum_{n=5}^{\infty}\left(\frac{Vn}{n^2}\right)^2} \qquad (11)$$

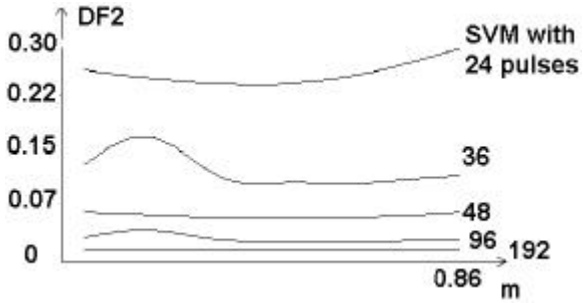

Fig.9 DF2 for regular SVM with different number of pulses on the fundamental period

V. VECTORIAL PWM

A. Theory

The three-phase inverter presented in Fig.2 is herein considered. Generally, the tip of the voltage Space Vector should follow a circular locus. This cannot be achieved by a switching power converter that is leading to discrete positions of the voltage Space Vector. Each desired position on the circular locus can be achieved by an average relationship

IEEE Copyright 2001

between two neighboring active vectors. Zero state vectors are used to fill-up the gap to a constant sampling interval.

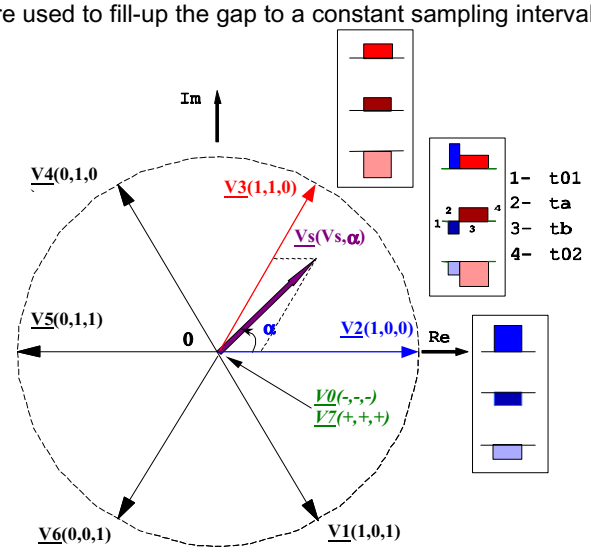

Fig.10 Generation of voltage Space Vector by SVM

$$\underline{V_S} \cdot T_S = \underline{V_a} \cdot t_a + \underline{V_b} \cdot t_b + \underline{V_0} \cdot t_0 \qquad (10)$$

where Ts= sampling period of the given circular locus (since usually the switching frequency is not equal with the carrier frequency, it is preferable to name T as sampling period); t_a, t_b =time intervals allocated to the neighboring vectors V_a, V_b. The meaning of the averaging process results from the LPF-ing action of the load at current derivation. Decomposition along ***Real*** and ***Imag*** axes yields:

$$\text{Re:} \quad V_S \cdot \cos\alpha \cdot T_S = \left(\frac{2}{3} \cdot V_d\right) \cdot t_a + \frac{1}{2} \cdot \frac{2}{3} \cdot V_d \cdot t_b \qquad (11)$$

$$\text{Im:} \quad V_S \cdot \sin\alpha \cdot T_S = 0 + \frac{\sqrt{3}}{2} \cdot \frac{2}{3} \cdot V_d \cdot t_b \qquad (12)$$

with the solution:

$$t_a = \frac{3\,V_s}{2\,V_d} \cdot T_S \cdot (\cos\alpha - \frac{1}{\sqrt{3}} \sin\alpha) = \frac{\sqrt{3}\,V_s}{V_d} \cdot T_S \cdot \sin(\frac{\pi}{3} - \alpha) \qquad (13)$$

$$t_b = \frac{\sqrt{3}\,V_s}{V_d} \cdot T_S \cdot \sin\alpha \qquad (14) \qquad t_0 = T_S - t_a - t_b \qquad (15)$$

In a digital implementation, these eqs. are usually carried based on a memory look-up table for the sine function within a 60 degrees interval or of the *sinα* and *sin(α–60)* within a 30 degrees interval. Alternative solutions are based on real-time interpolation of a minimized look-up table. This interpolation can be carried out by *Fuzzy Logic* as well.

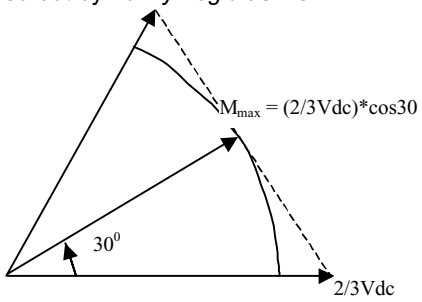

Fig.11 Definition of the maximum modulation index

Observing the time equations, one can derive the **maximum modulation index**. It will correspond to the circular locus with the maximum radius.

The presence of the **DC voltage** (V_d) in eq.(13-15) allows to compensate for the ripple of the DC bus voltage [18]. This ripple can be caused by the unsufficient filtering of the input rectifier power stage. Measuring the DC voltage at each sampling or with a larger sampling period will appropriately compensate for the effect of this ripple in the output voltage. Eq.(10) will keep account of a variable length of the active vectors (2/3Vd). However, this method reduces the maximum available voltage at the inverter output due to minimum Vd voltage within ripple. Equivalent compensation would also result with good current control loops but it is preferable to eliminate all the nonlinearities and parameter variations before closing the loop.

Eqs.(13-14) also show the dependence on the sampling period Ts (please note the nomenclature difference between sampling interval/sampling frequency and switching interval/ switching frequency). This allows using the same eqs. for **frequency modulation** by adjusting Ts [12.16,43]. It has been stated in the introduction that the presence of the zero-states can regulate the angular error and minimize the current/flux ripple. Several methods have been developed by using the sampling frequency as a degree of freedom in optimization after one or more criteria (low harmonics reduction, HCF reduction,s.o)., but all redefine Ts as:

$$T_S = \frac{1}{N \cdot f} \cdot (1 + \delta \cdot \cos(6 \cdot \alpha)) \qquad (16)$$

with N, number of intervals over the fundamental period (f). Regular methods have δ=0, while optimized ones require Ts shortened around 0 and 60 degrees but lengthened at 30 degrees. These ensure minimum angular errors, current distorsion factor at low harmonics and minimum torque pulsations [11]. Random Space Vector Modulation represents a special of frequency modulation.

B. Definition of the switching reference function

Directly using the time allocated to states given for (ta, tb) is sometimes not convenient for digital implementation. The definition of the switching sequence would result to be implemented in software only. It is more advantageous to define a function called "***Switching reference function***" with the same meaning as the reference used in sine-triangle comparison based PWM methods. It represents the duty ratio of each inverter leg or the conduction time normalized to the sampling period for a given switch and it is a mathematical function with variation between 0 and 1, centered around 0.5.

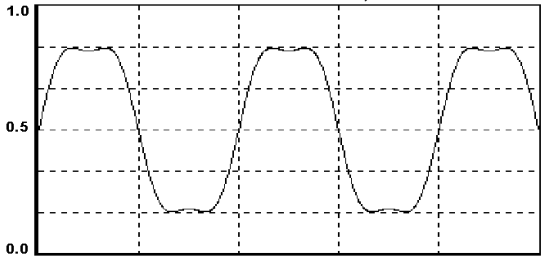

Fig.12 Reference function for the regular SVM

IEEE Copyright 2001

It can be derived by algebraic operations between the time intervals allocated to active and homopolar states within the same sampling interval. The Reference function for the regular Space Vector is shown in Fig.12 The difference between this function and a pure cosine reference is :

$$PW_{harm} = \begin{cases} 0.500 \cdot \sin\alpha, for \alpha \in (0,60) \\ 0.866 \cdot \cos\alpha, for \alpha \in (60,120) \\ -0.500 \cdot \sin\alpha, for \alpha \in (120,180) \end{cases} \quad (17)$$

A 3rd harmonic is present in the function but it is not present in the output phase or line voltages. It only represents the average of the A-M voltage from Fig.2.

$$v_{AB} = v_{AM} - v_{BM} \Rightarrow 3^{rd}\ harmonic\ \ vanishes \quad (18)$$

Similar methods of injecting the third harmonic in the reference waveform have been considered at sine-triangle intersection based methods. Maximization of the fundamental content led to a third harmonic of ¼of cosine reference, while the minimization of the HCF led to need of a third harmonic of 1/6 of the fundamental. There are papers [25,26,27,28,29] that analyzes this equivalence between regular sampled sine-triangle methods and SVM. They conclude that both methods are analogous and that conventional digital PWM controllers can be used for SVM generation in some cases.

Eqs.(13-15) do not provide a guide for sharing t_0 among the possible zero vector states. The initial SVM algorithm has taken advantage of this degree of freedom to reduce the number of switching processes by alternating the zero vector states. Moreover, the sharing has been considered as "*half-half*". The effect of considering different sharing ratio but the same original method of alternating zero-state vectors is shown by Figs.13 and 14 for a low number (=24) of intervals over fundamental [22,28]. At larger ratios, the differences will be smaller.

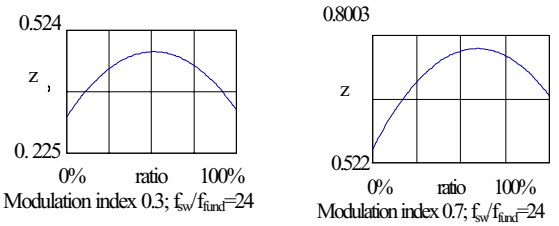

Fig.13 Effect of different sharing of the zero-states interval in content of fundamental

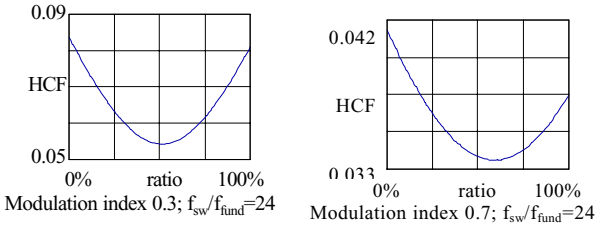

Fig.14 Effect of different sharing of the zero-states interval in HCF

These Figs. also show that the injection of the implicit third harmonic in the "*half-half*" SVM algorithm is close but not optimal for neither maximizing the fundamental content of phase voltage nor for minimization of the HCF. Actually, the amount of the third harmonic injected by SVM is about 0.22 (in between 1/4 and 1/6). For high-performance systems this can be further improved by a different placement of the zero-states within the sampling interval.

C. Link to Vector Control

This Space Vector Modulation algorithm provides the calculation of the pulse widths based on the polar co-ordinates (Vs,α). This is not very convenient for the Vector Control methods (both cases: drives and active filtering).

Sector 1 0..60 degrees	$t_a = \frac{3 \cdot T}{2 \cdot V_d} \cdot \left(v_x - \frac{1}{\sqrt{3}} \cdot v_y \right)$ $t_b = \frac{\sqrt{3} \cdot T}{V_d} \cdot v_y$	Sector 4 180..240 degrees	$t_a = \frac{3 \cdot T}{2 \cdot V_d} \cdot \left(-v_x + \frac{1}{\sqrt{3}} \cdot v_y \right)$ $t_b = \frac{-\sqrt{3} \cdot T}{V_d} \cdot v_y$
Sector 2 60..20 degrees	$t_a = \frac{3 \cdot T}{2 \cdot V_d} \cdot \left(v_x - \frac{1}{\sqrt{3}} \cdot v_y \right)$ $t_b = \frac{\sqrt{3} \cdot T}{V_d} \cdot \left(\frac{1}{2} \cdot v_y - \frac{\sqrt{3}}{2} \cdot v_x \right)$	Sector 5 240..300 degrees	$t_a = \frac{\sqrt{3} \cdot T}{2 \cdot V_d} \cdot \left(-v_x - 2 \cdot v_y \right)$ $t_b = \frac{\sqrt{3} \cdot T}{2 \cdot V_d} \cdot \left(-v_y + v_x \right)$
Sector 3 120..180 degrees	$t_a = \frac{T \cdot \sqrt{3}}{V_d} \cdot \left(v_y \right)$ $t_b = \frac{\sqrt{3} \cdot T}{2 \cdot V_d} \cdot \left(-v_y - \sqrt{3} \cdot v_x \right)$	Sector 6 300..360 degrees	$t_a = \frac{3 \cdot T}{2 \cdot V_d} \cdot \left(v_x - \frac{2 \cdot \sqrt{3}}{3} \cdot v_y \right)$ $t_b = \frac{\sqrt{3} \cdot T}{2 \cdot V_d} \cdot \left(v_y - \sqrt{3} \cdot v_x \right)$

Table I

VI. SELECTION OF THE SWITCHING SEQUENCE

The averaging principle used herein does not provide any requirement on zero vector generation during t_0. Moreover, the sequence of the active vectors within the sampling period is not unique and these degrees of freedom make the difference between Space Vector methods.

These eqs. are employed to redefine the eqs. for (*ta,tb*). The time intervals allocated to the zero vectors remains

$$t_0 = T_S - t_a - t_b \quad (32)$$

The methods to be presented in the followings are named in different ways by different researchers. To simplify the

IEEE Copyright 2001

explanation, the names of methods used herein are chosen for this tutorial only.

A Continuous Reference Function

- **Direct-Inverse SVM [8,9]**

To reduce the number of the inverter switchings, it is necessary to distribute the switching sequence in such a way that the transition from one state to the next is performed by switching only one inverter leg at a time. This results in starting the sampling period with one zero state and ending at the other state. For instance, if the desired vector is in the first sector of Fig.10, the switching sequence has to be …0237320… The only remaining degree of freedom consists in the way we are sharing t_0 between the vectors $\underline{V_0}$ and $\underline{V_7}$. The two extreme situations are:

Method DIH - equal sharing of the zero vector intervals on each sampling interval (t_0=t_7) [9,19,20,21]:

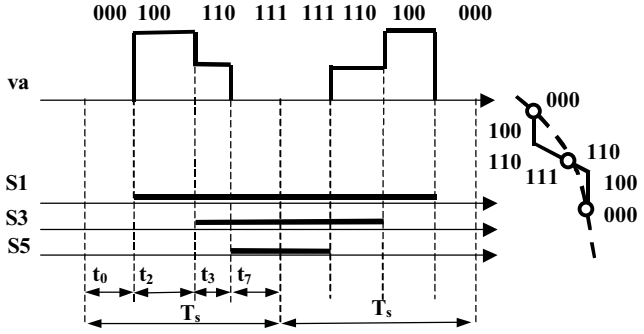

Fig.15 Pulse generation with Method DIH

Method DIO: - use of only a zero vector interval within each sampling period (Ex: t_0=0, t_7=T_s-t_a-t_b):

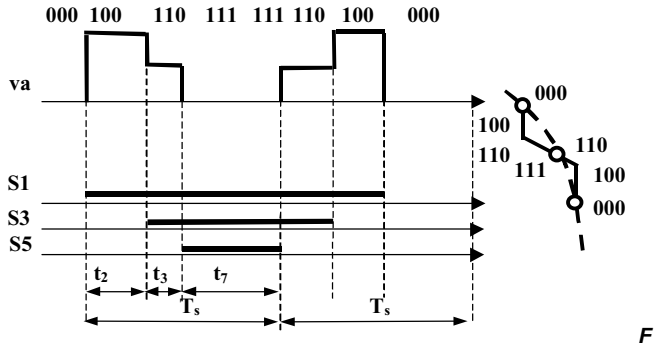

ig.16 Pulse generation with Method DIO

The time intervals allocated to the homopolar component can be shared in different ways between $\underline{V_0}$ and $\underline{V_7}$ and the way we are placing the active states within the sampling period influences the content in fundamental or the Total Harmonic Distortion coefficient. Equal sharing provides a good compromise between simplicity and HCF/z performance.

Method DIO can be used only at high sampling frequencies, otherwise important even harmonics are present in the output phase voltage since the waveform symmetries are not longer respected. On the other hand, if the sampling frequency is large enough, the spectral differences between the voltages carried out by ***Method DIH*** or ***Method DIO*** will be very reduced.

Both methods presented determine three switchings/ sampling period.

- **Simple Direct SVM**

A simple way to synthesize the output voltage vector is to turn-on all the switches connected to the same DC link busbar at the beginning of the switching cycle and to turn off sequentially in order to split the zero vector interval between $\underline{V_0}$ and $\underline{V_7}$ (t_0=t_7)

Method SDH: This method is similar to usual sine-triangle comparison based PWM.

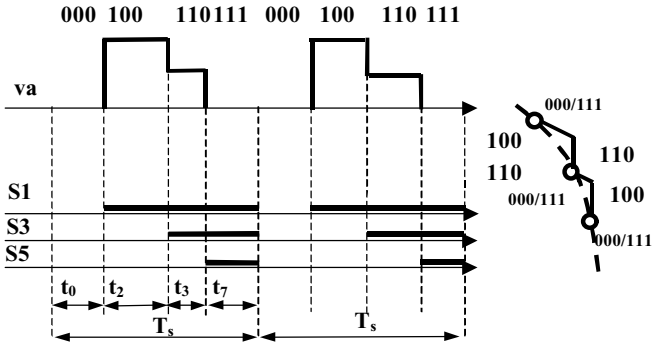

Fig.17 Pulse generation with Method DIO

- **Symmetrically Generated SVM [ ]**

This modulation scheme is based on symmetrical sequence within each sampling period. It looks like "*Direct-Inverse"* methods but the direct-inverse sequence are inside the sampling period. Even if it looks unnecessarily complicated, this method presents the advantage of a direct implementation on the existing PWM IC working on the basis of center-aligned PWM.

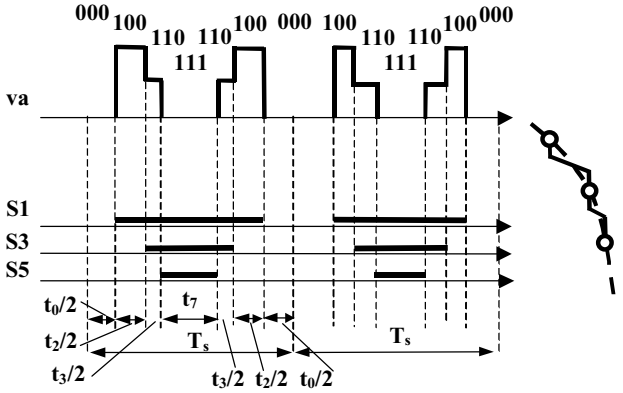

Fig.18 Pulse generation with Method SGS

B. Discontinuous Reference Function [30-39] for achieving reduced switching loss

The previous studies over the regular-sampled PWM algorithms have demonstrated the advantages of discontinuous algorithms to reducing the inverter switching loss [30-34]. The same idea has been carried out using the Space Vector Modulation algorithm as support [35-41].

IEEE Copyright 2001

Any two neighboring vectors are different by a switching in an inverter leg only. This can be used to minimize the number of the switching processes by employing only one zero-vector on each sector. No switchings on an inverter leg within the respective sector results. It yields two possible state sequence for each generation of a desired vector:

Method DZ0: The null vector is always fixed as [0 0 0]

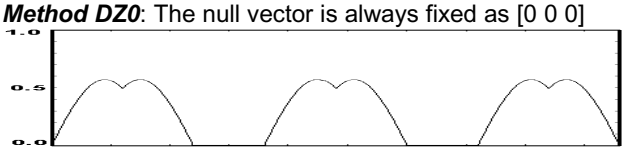

Fig.19 Method DZ0

Method DZ1: The null vector is always fixed as [1 1 1]

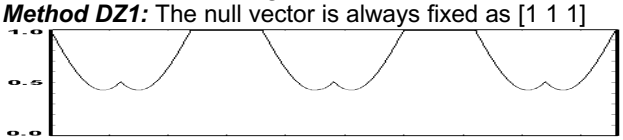

Fig.20 Pulse generation with Methods DZ0 and DZ1

Within these methods, three power switches are "*on*" for extended periods of time and this may create a problem in inverter bridges that use isolation circuits such as the boot-strap. That is why they are not used in industry. To obtain a symmetrical stress of the power devices, the degree of freedom consists in choosing a 60 degrees interval within 120 degrees. For instance, one can keep the first phase without any switching from –60 to 60 degrees (Vectors "110" and "100" in *Sector 1* ; "100" and "101" in *Sector 6*), but only a 60 degrees interval is actually inside *Sector 1* and/or *Sector 2*.

Switching loss is approximately proportional to the magnitude of the current being switched and it would be advantageous to avoid switching the inverter leg with the highest instantaneous current.

Method DD1: Null vector [1 1 1] is assigned for sectors 1,3,5 and null vector [0 0 0] is assigned for sectors 2,4,6. The no-switching interval occurs in the 60 degrees next after the peak of the phase voltage. Generally, the current is lagging the phase voltage and most probably the peak of the current fundamental sits in the next 60 degrees after the peak of voltage. This method reduces the switching loss.

Method DD2: The 60 degrees no-switching interval is chosen around the peak of the fundamental of voltage. This method is very useful to reduction of the switching losses in AC/DC converters where the power factor is desirable unity and the peak of current is nearby the peak of voltage.

Method DD3: No-switchings around the measured peak of the phase current. This means equally spreading the 60-degrees no-switching interval around the peak of the phase current. However, if the phase current and voltage out of phase is greater than 30 degrees, the 60-degrees no-switching region will overcame the vector sector. If for instance, the voltage vector is V2 and the current vector is at 50 degrees, equally partitioning the no-switching region for the first inverter leg around the current vector would lead to an area between 20 and 80 degrees. For α>60, keeping the first phase on "1" is no longer possible since the Sector2 is characterized by switchings on the first phase. We can look after no switchings in the other 2 phases but the other currents are lower and the merits of the method are compromised [40].

Methods DZ1, DZ2, DD1, DD2, DD3 can be implemented by using a direct-direct sequence:

$$| V_{A1} - V_{A2} - V_Z \;|\; V_{A1} - V_{A2} - V_Z |$$

or a direct-inverse sequence

$$| V_{A1} - V_{A2} - V_Z \;|\; V_Z - V_{A2} - V_{A1} |$$

when the number of switchings is reduced by half as demonstrated before.

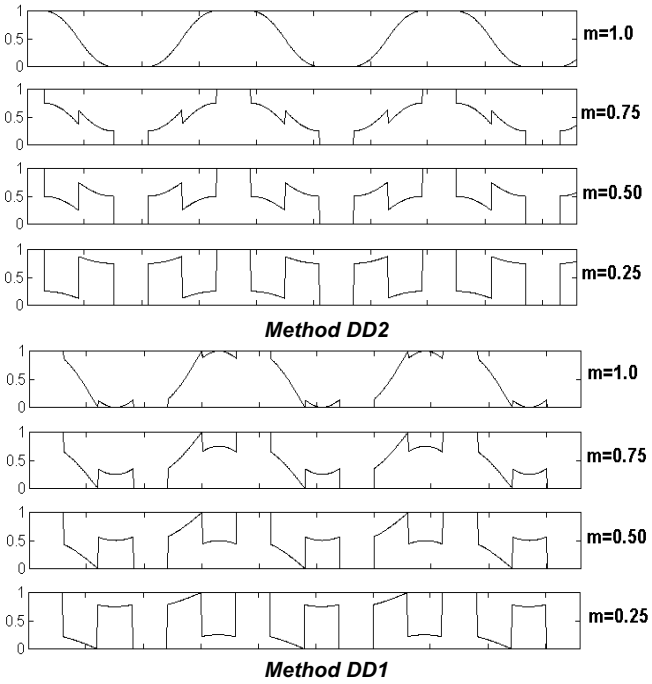

Fig.21 Pulse generation with Methods DD1 and DD2 for different modulation indices

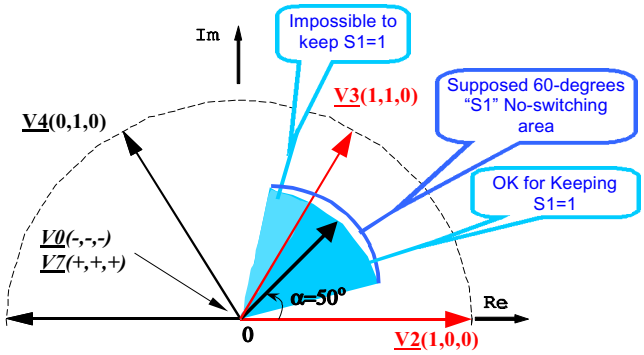

Fig.22 Vectorial discussion around the DD3 Method

VII. COMPARISON BETWEEN DIFFERENT CHOICES

A. Understanding performance of discontinuous reference waveforms

Previous section has shown that the two active and zero states can be placed within the sampling period in different ways providing advantages in reduction of the number of switching processes or in moving the switchings at lower load current levels. At this point, someone can ask how much reduction of the switching loss can be achieved by discontinuous methods. Fig.22 answers this question by presenting the switching power with discontinuous PWM

IEEE Copyright 2001

method normalized to the switching power with continuous PWM algorithms versus load power angle. The results are based on a theoretical analysis considering the load current level at each switching and the number of the switching processes. The best case leads to 50% savings in switching loss [40-42].

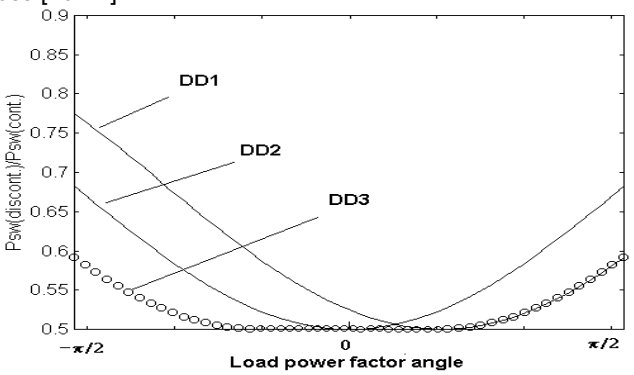

Fig.23 Switching power with discontinuous PWM normalized to the switching power with continuous PWM algorithms versus load power angle

If the results are so outstanding, why the discontinuous methods are not always used? Using discontinuous PWM methods can introduce oscillations (glitches) at the points when the sector is changed due to different time interval equations for each sector. This is much clear at low output frequencies and it increases the loss in the load and may introduce instabilities of the control system. More important, additional differences in current quality will be shown in the followings.

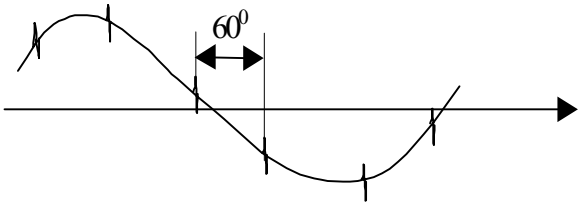

Fig.24 Possible output phase current when applying discontinuous PWM algorithms

B. Comparison of switching behaviour

=The difference between the conduction loss among the SVM techniques is less than 3% of the total loss. Switching performance is shown by **Table II.**

C*. Quality of the current waveforms*

Choosing different state sequence over a given sampling interval preserves the same average value of phase voltages. However, different ripple levels could result in the current waveforms. This can be understand by inspecting the current trajectories in the complex plane shown along with definition of different SVM methods. Fig.24 shows current distorsion factor comparative results for different SVM methods.

Method	No.switchings Within Ts	THDv	Dominant Harmonics		No. states
Direct-Inverse ***(DIH)***	3		Fs/2		4
Direct Inverse ***(DIO)***	3		Fs/2		3
Simple Direct ***(SDH)***	6		Fs		4
Symmetric Gen. ***(SGS)***	6	least	Fs		7
Direct-direct/000 ***(DZ0)***	4		Fs		3
Direct-direct/111 ***(DZ1***)	4		Fs		3
Direct-direct/sect ***(DD1)***	4/2		Fs		3
Direct-direct/peak ***(DD2)***	4/2		Fs		3
Direct-direct/mes ***(DD3)***	4/2		Fs		3

Table II

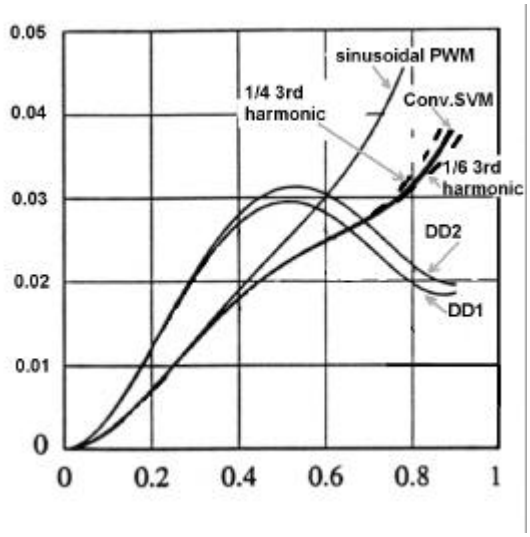

Fig.25 Distortion factor vs modulation index

VIII. Conclusion

The theory of the Space Vector Modulation for a 3-phase inverter is presented by this tutorial. This theory has been further extended to other 3-phase converter systems and nowadays became a standard for industry.

REFERENCES

[1] Park, R.H., "Two-Reaction Theory of Synchronous Machines", AIEE Trans. No.48, 1929, pp.716-730 and no. 52, 1933, pp.352-355.
[2] Kron, G., "The Application of Tensors to the Analysis of Rotating Electrical Machinery", Schenectady, NY, USA, General Electric Review, 1942
[3] Kovacs, K.P., Racz, I., "Transiente Vorgange in Wechselstrommachinen", Budapest, Hungary, Akad.Kiado, 1959
[4] Stepina, J., "Raumzeiger als Grundlage der Theorie der Elktrischen Maschinen", etz-A, 88, no.23, 1967, pp.584-588
[5] L.Serrano, Iribarnegaray, "The Modern Space Vector Theory, Part I: Its Coherent Formulation and Its Advantages for Transient Analysis o Converter-Fed AC Machines", ETEP, vol.3, no.2, March/April, 1993,
[6] W.Leonhard, "30 years of Space Vector, 20 Years Field Orientation, 10 Years Digital Signal Processing with Controlled AC-Drives, A Review", EPE Journal, vol. , no. 1-2, 1991 (I & II)

IEEE Copyright 2001

[7] Y.Murai, Y.Tsunehiro, "Improved PWM Method for Induction Motor Drive Inverters", IPEC, Tokyo, 1983, pp.407-417
[8] J. Holtz, P.Lammert, W.Lotzkat, "High-speed drive system with ultrasonic MOSFET PWM Inverter and Single-chip Microprocessor Control", Conf.Rec. 1986 IEEE-IAS Ann.Mtg., pp.12-17
[9] Van der Broeck, Skudelny, H.C., Stanke, G.: "Analysis and Realisation of a Pulse Width Modulator Based on Voltage Space Vectors", Conf.Rec. 1986 Annual Meeting IEEE-IAS, Denver/USA, pp.244-251.
[10] V.H.Prasad, D.Borojevic, S.Dubovsky, "Comparison of High-Frequency PWM Algorithms for Voltage Source Inverters", …
[11] Y.Iwaji, S.Fukuda, "A Pulse Frequency Modulated PWM Inverter for Induction Motor Drive", IEEE Transactions on PE, vol.7, no.2, April 1992
[12] Y.Murai, Y.Gohshi, K.Matsui, I.Hosono, "High-Frequency Split Zero-Vector PWM with Harmonic Reduction for Induction Motor Drive", Trans.on IA, vol.28, no.1, Jan/Feb. 1992, pp.105-112
[13] Murai, Y., Sugimoto S., Iwasaki, H., Tsunehiro Y.: "Analysis of PWM Inverter Fed Inductions Motors for Microprocessors", Proc.IEEE/IECON,1983,pp.58-63
[14] Fukuda, S., Iwaji, Y., Hasegawa H.: "PWM Technique for Inverter with Sinusoidal Output Current", IEEE Trans. on Power Electronics, no.5, 1990, pp.54-61
[15] E.Ch.Andersen, A.Hann, "Influence of the PWM Control Method on the Performance of Frequency Inverter Induction Machine Drives", ETEP, vol.3, no.2, March/April 1993, pp.151-160
[16] J.Holtz, "Pulsewidth Modulation – A Survey", IEEE Trans. On IE, vol.39, no.5, Dec.1992, pp.410-420
[17]J.Holtz, "Pulsewidth Modulation for Electronic Power Conversion", Proc.of the IEEE, vol.82, no.8, August 1994, pp.1194-1212
[18] P.Enjeti, A.Shireen, "A New Technique to Reject DC-Link Voltage Ripple for Inverters Operating on Programmed PWM Waveforms", IEEE Trans. on PE, vol.7, no.1, Jan.1992, pp.171-180
[19] Granado, J., Harley, R.G., Diana G.: "Understanding and Designing a Space Vector Pulse-Width-Modulator to Control a Three Phase Inverter", . Trans. of the SAIEE (1989), vol.80, Sept.1989, pp.29-37
[20] Palma, C.P.J., Santana J.E.Joao, "Vectorial PWM Methods, Implementation and Results for some AC-AC Converter Structures", Conf.Rec. Medit. Electr. Conf. "Melecon'91", Ljubliana, May 22-24 1991, pp.1388-1401
[21] Lucanu, M., Neacsu, D., "Optimal U/f Control for Space Vector PWM Three-Phase Inverters", European Transactions on Electrical Power Eng., vol. 5, no. 2. March/April, 1995, pp. 115-120
[22] Dorin Neacsu, "A New Digital Controller for SVM Algoritm", IEEE, SCS '93, Nov. 4-5, 1993, pp. 256-259
[23] Dorin Neacsu, M. Lucanu, "Output Waveform Optimization of the SVM Inverters", Proc. Of National Conference Electrical Drives, Iasi, Romania, Oct. 22-24, 1992, pp.B1-B6
[24] Dorin Neacsu, D. Alexa, "Analysis of High-Frequency PWM Techniques Suitable for Resonant Inverters", ETEP, vol. 6, no. 3, May/ June, 1996, pp. 183-188
[25] Y-S Lai; Bowes, S.R., "A universal Space Vector modulation strategy based on regular-sampled pulse-width modulation [invertors]", Proc. of the 1996 IEEE IECON 22nd, Vol.1 , pp. 120 - 126
[26] Bowes, S.R.; Yen-Shin Lai, "The relationship between space-vector modulation and regular-sampled PWM", IEEE Trans. on Industrial Electronics, vol. 44 5 , pp. 670 -679
[27] Jian Sun; Grotstollen, H. ,"Optimized Space Vector modulation and regular-sampled PWM: a Reexamination, Conf.Rec. of IEEE IAS '96., vol.2 , pp. 956 –963
[28] Holmes, D.G , "The significance of zero Space Vector placement for carrier based PWM schemes", Conf. Record of the 1995 IEEE IAS, vol.3 , pp. 2451 -2458
[29] Holmes, D.G., "The general relationship between regular-sampled pulse-width-modulation and space vector modulation for hard switched converters", IAS Annual Meeting, 1992., Conf.Record 1992 IEEE , pp 1002 -1009 vol.1
[30] J.W.Kolar, H.Ertl, F.C.Zach, "Calculation of the Passive and Active Component Stress of Three-Phase PWM Converter", Proc.EPE 1989, pp.1303-1311
[31] D.R.Alexander, S.M.Williams, "An optimal PWM algorithm implementation in a High Performance 125kVA Inverter", Proc.APEC 1993, pp.771-777
[32] H.van der Broeck, "Analysis of the Harmonics in Voltage-Fed Inverter Drives Caused by PWM Schemes with Discontinuous Switching Operation", Proc.EPE'91, pp.3/261-3/266
[33] J.A.Houldsworth, D.A.Grant, "The Use of Harmonic Distortion to Increase the Output Voltage of a Three-Phase PWM Inverter", IEEE trans. on IA, vol.IA-20, 1084, pp.1224-1228
[34] A.M.Hava, R.J.Kerkman, T.A.Lipo, "A High Performance Generalized Discontinuous PWM Algorithms" APEC'97, vol.2, pp.886-894
[35] A.M.Trzynadlowski, S.Legowski, "Minimum-Loss Vector PWM Strategy for Three-Phase Inverters", IEEE Trans. on PE, vol.9, no.1, Jan.1994, pp.26-34
[36] D.W.Chung, S.L.Sul, "Minimum-Loss PWM Strategy for a 3-Phase PWM Rectifier", PESC 1997, vol.2, pp.1020-1026
[37] R.S.Lai, K.D.T.Ngo, "A PWM Method for Reduction of switching Loss in a Full-Bridge Inverter", IEEE Trans.on PE, May 1995, vol.10, no.3, pp.326-332
[38] A.M.Trzynadlowski, R.L.Kirlin, S.Legowski, "Space Vector PWM Technique with Minimum Switching Losses and a Variable Pulse Rate", IEEE Trans. on IE, April 1997, vol.44, no.2, pp.173-181
[39] E.Faldella, C.Rossi, "High-Efficiency PWM techniques for Digital Control of DC/AC Converters", APEC 1994, vol.I, pp.115-121
[40] Dorin Neacsu, K.Rajashekara, F.Gunawan, "Overmodulation for Zero Switching Modulation", Research Disclosure, GM, 1997
[41] Perruchoud, P.J.P.; Pinewski, P.J. , "Power losses for Space Vector modulation techniques ", Power Electronics in Transportation, 1996., IEEE , pp. 167 –173
[42] R.H.Ahmad, G.G.Karady, T.D.Blake, P.Pinewski, "Comparison in Space Vector Modulation techniques Based on Performance Indexes and Hardware Implementation", IEEE IECON 97, 23rd Intl.Conference, vol.2 , pp. 682 –687
[43] Dorin Neacsu, V.Donescu, C.Neacsu, "Analysis, simulation and modeling of power converters", 1999, Ed.Asachi, Iasi, Romania

Dorin O. Neacsu *(M'95, SM'00) was born in Suceava, Romania, in 1964. He received the MS and PhD degrees in electrical engineering from the Technical University of Iasi, Iasi, Romania, in 1988 and 1994, respectively. He was with TAGCM-SUT Iasi, Romania, from 1988 to 1990. Since 1990, he has been with the faculty of the Department of Electronics, Technical University of Iasi.*

In 1995, he has been a Post-Doctoral Fellow at Universite du Quebec a Trois Rivieres, Canada. Between February 1997 and August 1998, he has been at Delphi-Energy and Engine Management Systems, Indianapolis, USA, working on advanced DSP control of electrical drives for propulsion systems. In August 1999, he joined International Rectifier, in El Segundo, CA, USA. Since January 2001, Dr.Neacsu has joined Satcon Corp., in Cambridge, MA, USA. Along with many papers or research notes published in journals or conference proceedings, Dr. Neacsu has co-written several university textbooks in Canada and Romania and a book on simulation-modelling of power converters in Romanian language. Dr. Neacsu has served as a Reviewer or Session Chairman for several IEEE conferences. His research areas are in static power converters, PWM algorithms, microprocessor control, modeling and simulation of power converters and emerging control technologies as fuzzy logic.

IEEE Copyright 2001